Available online at www.sciencedirect.com

SCIENCE DIRECT®

ELSEVIER

Microporous and Mesoporous Materials 90 (2006) 314–326

MICROPOROUS AND MESOPOROUS MATERIALS

www.elsevier.com/locate/micromeso

Sites for CO_2 activation over amine-functionalized mesoporous Ti(Al)-SBA-15 catalysts

R. Srivastava, D. Srinivas, P. Ratnasamy *

National Chemical Laboratory, Homi Bhabha Road, Pune 411 008, India

Received 16 May 2005; received in revised form 26 October 2005; accepted 26 October 2005
Available online 15 December 2005

Dedicated to the late Denise Barthomeuf, George Kokotailo and Sergey P. Zhdanov in appreciation of their outstanding contributions to zeolite science

---

Abstract

Activation of CO_2 and its utilization in the synthesis of chloropropene and styrene carbonates over functionalized, mesoporous SBA-15 solids, have been investigated. The surface basicity of SBA-15 was modified with nitrogen-based organic molecules of varying basicity viz., alkyl amines (–NH_2), adenine (Ade), imidazole (Im) and guanine (Gua). The surface of SBA-15 was also functionalized with Ti^{4+} and Al^{3+} species. The acid–base properties of these modified SBA-15 materials were investigated by temperature-programmed desorption (TPD) and diffuse-reflectance infrared Fourier transform (DRIFT) spectroscopy. NH_3 and pyridine were used as probe molecules for acid sites, while CO_2 was used to characterize the basic sites. CO_2 was activated at the basic amine sites forming surface carbamate species (IR peaks: 1609 and 1446 cm^{-1}). The latter reacted further with epoxides adsorbed on the acid sites forming cyclic carbonates. A correlation between the intensity of the IR peak at 1609 cm^{-1} and cyclic carbonate yield has been observed. The cyclic carbonate yields were higher when both the acid and base functionalities were present on the surface. The Ti- and Al-SBA-15 functionalized with adenine exhibited the highest catalytic activity and selectivity. There is an optimal dependence ("volcanic plot") of the yield of cyclic carbonates on the desorption temperature, $T_{max}(CO_2)$ in the TPD experiments. These solid catalysts were structurally stable up to 473 K and could be recycled for repeated use. In addition to density, the strength and type of amine sites play a crucial role on CO_2 activation and utilization.

Keywords: CO_2 activation; CO_2 utilization; Chemical fixation of carbon dioxide; Active sites; Chemicals from CO_2; Amine-functionalized mesoporous SBA-15, Ti-SBA-15 and Al-SBA-15

1. Introduction

Greater utilization of CO_2 as a renewable *raw* material in the chemical industry is an area of current interest. At present, CO_2 is used in the manufacture of urea, salicylic and *para*-hydroxy benzoic acids, methanol and cyclic carbonates. Its increased use is feasible only if this thermodynamically stable and kinetically inert molecule can be activated for reactions [1–6]. CO_2 can be activated by coordination to a transition metal center [5]. It can also be activated, by binding with a base (like HO^-) [7,8]. Since the rate-determining step in most of the reactions involving CO_2 is the initial activation of the CO_2 molecule, coordination with a transition metal center or a base lowers the activation energy required in further reactions involving the CO_2 molecule and thereby makes it possible to convert this inert molecule with suitable reactants into useful products. While the activation of CO_2 by metal complexes has been investigated in detail (see for example Ref. [5]), the mechanism of CO_2 activation by bases, and, especially, solid bases is not so well explored. The use of solid instead of homogeneous base catalysts in the insertion of CO_2 in

---

* Corresponding author. Tel.: +91 20 2590 2018; fax: +91 20 2589 3761.
E-mail address: p.ratnasamy@ncl.res.in (P. Ratnasamy).

1387-1811/$ - see front matter © 2005 Elsevier Inc. All rights reserved.
doi:10.1016/j.micromeso.2005.10.043

phenols (to yield *ortho-/para*-hydroxy benzoic acids) or oxiranes (to yield cyclic carbonates) or amines (to yield carbamates) will lead to environmentally more benign processes for the manufacture of chemicals using CO_2 as a raw material.

We have recently reported the application of heterogeneous catalysts in the synthesis of carbonates and carbamates [9–14] in high yields avoiding the use of solvents and co-catalysts/promoters (which are usually used with homogeneous catalysts) under mild reaction conditions. Molecular sieves, like SBA-15 or Ti-SBA-15 whose surface (OH) groups have been functionalized with amines, like adenine, were excellent catalysts in the activation of CO_2 and its subsequent insertion in organic substrates to yield carbonates and carbamates [14]. In the present study, we explore the nature of the active sites on these catalysts using in situ IR spectroscopy of adsorbed CO_2 molecules and thermal desorption techniques. The important role of surface basic sites in the binding and activation of CO_2 is demonstrated.

2. Experimental

2.1. Materials preparation

2.1.1. Preparation of SBA-15

SBA-15 was prepared [15,16] using tetraethyl orthosilicate (TEOS, Aldrich Co.) as a silica source, Pluronic P123 (amphiphilic tri-block co-polymer, poly(ethylene glycol)-block-poly(propylene glycol)-block-poly(ethylene glycol), $EO_{20}PO_{70}EO_{20}$; average molecular weight = 5800, Aldrich Co.) as a template and HCl to control the pH. In a typical synthesis, 2 g of P123 was dispersed in 15 g of water and 60 g of 2 M HCl solution while stirring. To the, resultant homogeneous solution, was added 4.25 g of TEOS. This gel was continuously stirred at 313 K for 24 h and aged at 373 K, for 2 days. Then the solid product was separated by centrifugation, washed with deionized water, and dried at 298 K. The material was finally calcined in air, at 823 K for 6 h to decompose the triblock co-polymer and to obtain a white powder, SBA-15.

2.1.2. Preparation of Ti-SBA-15

Ti-incorporated SBA-15 (Ti-SBA-15) was prepared by a post-synthesis method [16] using tetrabutyl orthotitanate (95 wt% TBOT, Aldrich Co.) as Ti source. In a typical preparation, a certain amount of TBOT (0.566 g for Si/Ti = 40, for example) was hydrolyzed in 40 cm^3 of glycerol (99 wt%, s.d. fine Chem. Ltd.) containing 7.5 cm^3 of tetrapropylammonium hydroxide (TPAOH; 20 wt%, Aldrich Co.), to obtain a homogeneous solution. To this solution was added 2 g of SBA-15, and the mixture was heated statically at 373 K for 72 h. Ti-SBA-15, thus obtained, was filtered, washed with deionized water, and the organic species were burnt off in air at 773 K for 4 h. The material used in the present study contained a final Si/Ti composition of 40.

2.1.3. Preparation of Al-SBA-15

In a typical preparation [17], 4 g of P123 was dissolved in 30 cm^3 of water. After stirring for 4 h at 298 K a clear solution was obtained. To that, 1.75 g of HCl diluted in 70 cm^3 of distilled water was added. The solution was stirred for 2 h at 313 K and then 9 g of TEOS and 1.26 g of aluminum isopropoxide (input Si/Al = 7) were added to it and the stirring was continued to another 20 h at 313 K. The gel was aged at 373 K for 48 h. The solid obtained was filtered, washed thoroughly with distilled water and then calcined at 773 K for 4 h to obtain Al-SBA-15 with a final Si/Al composition of 22.

2.1.4. Preparation of SBA-15-pr-Cl, SBA-15-pr-NH_2, Ti-SBA-15-pr-Cl, Ti-SBA-15-pr-NH_2 and Al-SBA-15-pr-Cl

SBA-15 was activated under vacuum at 423 K for about 3 h. 3-Chloro or 3-aminopropyltriethoxysilane (9 mmol per 3 g of SBA-15; Lancaster) in 100 cm^3 of dry toluene was then added and refluxed under nitrogen for 6 h [18,19]. Soxhlet extraction, first with dichloromethane (for 12 h) and then with acetone (for 12 h) yielded Cl- and NH_2-functionalized SBA-15 materials, SBA-15-*pr*-Cl and SBA-15-*pr*-NH_2, respectively. Ti-SBA-15-*pr*-Cl, Ti-SBA-15-*pr*-NH_2 and Al-SBA-15-*pr*-Cl were prepared in a similar manner using Ti-SBA-15 and Al-SBA-15 in place of SBA-15.

2.1.5. Preparation of SBA-15-pr-Im and Ti-SBA-15-pr-Im

Imidazole (3 mmol, 0.204 g) was taken in 30 cm^3 of dry $CHCl_3$ and stirred for 30 min under nitrogen environment at reflux temperature for complete dissolution. Then, 1.5 g of SBA-15-*pr*-Cl or Ti-SBA-15-*pr*-Cl was added and stirring was continued for 12 h. The solid was filtered, Soxhlet extracted first with $CHCl_3$ (for 10 h) and then with CH_3CN (for 12 h).

2.1.6. Preparation of SBA-15-pr-Gua and Ti-SBA-15-pr-Gua

Guanine (1.76 mmol, 0.266 g) was taken in 30 cm^3 of dry DMF and stirred for 30 min under nitrogen environment at 393 K for complete dissolution. Then, 1.5 g of SBA-15-*pr*-Cl or Ti-SBA-15-*pr*-Cl was added and stirring was continued for 12 h. The solid was filtered, Soxhlet extracted first with DMF (for 10 h) and then with CH_3CN (for 12 h).

2.1.7. Preparation of SBA-15-pr-Ade, Ti-SBA-15-pr-Ade and Al-SBA-15-pr-Ade

Adenine (1.76 mmol, 0.238 g) was taken in 30 cm^3 of dry DMF and stirred for 30 min under nitrogen environment at 393 K for complete dissolution. Then, 1.5 g of SBA-15-*pr*-Cl or Ti-SBA-15-*pr*-Cl or Al-SBA-15-*pr*-Cl was added and stirring was continued for 12 h. The solid was filtered, Soxhlet extracted first with DMF (for 10 h) and then with CH_3CN (for 12 h).

2.2. Materials characterization

X-ray diffractograms were recorded on an X'Pert Pro (Philips) diffractometer using Cu Kα radiation and a proportional counter as detector. A divergence slit of 1/32° on the primary optics and an anti-scatter slit of 1/16° on the secondary optics were employed to measure the data in the low angle region. Transmission electron microscopy of the samples was done on a JEOL (model 1200 EX) microscope operating at 100 kV. The calcined sample was dispersed in isopropyl alcohol, deposited on a Cu grid and dried. Ti-content in titanium-containing SBA-15 samples was estimated using a Rigaku 3070 E wavelength dispersive X-ray fluorescence (XRF) spectrometer with Rh target energized at 50 kV and 40 mA. Al-content in Al-SBA-15 and Al-SBA-15-*pr*-Ade was estimated by EDAX. The C, H & N composition was estimated by a Carlo-Erba 1106 analyzer. The specific surface area of the samples was determined by BET method using a NOVA 1200 Quanta Chrome equipment and the data points of p/p_0 in the range of about 0.05–0.3. The micropore volume was determined from the *t*-plot. The reference alumina sample supplied by Quanta Chrome was used for calibrating the instrument. The pore diameter was estimated using the Barret–Joyner–Halenda (BJH) model. Thermogravimetric analysis was done on a Seiko DTA-TG 320 instrument under air (50 cm^3/min), at a ramp rate of 10 K/min, in the temperature range of 308–1078 K. Solid state ^{27}Al MAS NMR spectra were recorded at 298 K on a Bruker MSL 300 spectrometer. Samples were spun at 10 kHz using a 4 mm diameter zirconia rotor. In CO_2 adsorption studies using FT-IR spectroscopy (Shimadzu 8201 PC spectrophotometer in the region 400–4000 cm^{-1}), the samples were made into a paste with dichloromethane and then exposed to CO_2 (20 bar) at 253 K for 1 h. The spectra, before and after CO_2 adsorption, were recorded in diffuse reflectance mode (spectral resolution = 4 cm^{-1}; number of scans = 100) and the difference spectrum obtained (by subtracting the spectrum of the unexposed SBA-15 sample from that of the corresponding CO_2 adsorbed sample) is used for further analysis.

The FT-IR spectra of adsorbed pyridine on different samples were recorded with a Shimadzu SSU 8000 DRIFT spectrophotometer equipped with a liquid-nitrogen cooled MCT detector. Samples were activated at 573 K for SBA-15 and Ti-SBA-15 and at 473 K for those containing the organic functionality. They were, then, cooled to 323 K and pyridine (0.03 cm^3) was adsorbed. The sample temperature was raised and held at the desired value for 30 min before recording the spectrum (spectral resolution = 4 cm^{-1}; number of scans = 100). Difference spectra were obtained by subtracting the spectrum of the catalyst from that of the corresponding pyridine-adsorbed samples. Diffuse-reflectance UV–visible (UV–Vis DRS) spectra were obtained on a Shimadzu spectrophotometer (UV-2500 PC).

Temperature-programmed desorption (TPD) experiments were conducted on a Micromeritics AutoChem 2910 instrument. In a typical experiment, ca. 120 mg of sample was taken in a U-shaped, flow-through, quartz sample tube. Prior to the TPD experiments, the catalyst was pretreated in He (50 cm^3/min) at 473 K for 1 h. A mixture of NH_3 in He (10:90) was then passed (75 cm^3/min) at 353 K for 1 h. The sample was, subsequently flushed in He (50 cm^3/min) at 383 K for 2 h to remove physisorbed ammonia. The TPD experiments were carried out in the range of 323–623 K at a heating rate of 10 K/min. The ammonia concentration in the effluent was monitored with a gold-plated, filament thermal conductivity detector. The peaks were integrated using the software GRAMS/32 to determine the amount of ammonia desorbed.

In CO_2-TPD experiments the catalyst was pretreated at 473 K for 1 h. CO_2 was adsorbed at 300 K for 1 h. The sample was, then, flushed for 1 h to remove physisorbed CO_2. The TPD was conducted from 298 K to 523 K at a heating rate of 10 K/min. The sample was then kept at 523 K for 30 min.

2.3. Catalytic activity

A typical catalytic activity reaction was conducted taking 18 mmol of epoxide (epichlorohydrin or styrene oxide) and 100 mg of solid catalyst in a stainless steel PARR reactor. The reactor was pressurized with CO_2 (6.9 bar), the temperature was raised to 393 K and the reaction was carried out for a specific period of time. Finally, the reactor was cooled to 298 K, unreacted CO_2 was vented out, the catalyst was separated and the products were isolated and analyzed by gas chromatography (Varian 3400; CP-SIL8CB column; with a 30 m-long, and 0.53 mm-i.d.). The products were identified by GC–MS (Shimadzu QP-5000; with a 30 m-long, 0.25 mm-i.d., and 0.25 μm-thick capillary column DB-1), GC-IR (Perkin–Elmer 2000; BP-1 column; with a 25 m-long, and 0.32 mm-i.d.) and ^{1}H NMR (Bruker AC 200).

3. Results and discussion

3.1. Catalyst characterization—structural properties

Mesoporous SBA-15 was functionalized with various acidic and basic functionalities. The acidic functionalities were Lewis acid Ti^{4+} and Al^{3+}. Basicity of SBA-15 was varied systematically by covalently anchoring primary-, secondary- and tertiary amine-containing organic bases viz., alkyl amine (–NH_2), adenine (ade), imidazole (–Im) and guanine (–Gua).

3.1.1. XRD

The low-angle X-ray diffraction profiles of SBA-15 and its functionalized derivatives showed reflections in the 2θ range of 0.8–2° (Fig. 1) attributable to 2D hexagonal *p6mm* symmetry [16]. The well-resolved (1 1 0) and (2 0 0) reflections reveal long-range mesopore ordering of the SBA-15 materials. The *d* spacing (d_{100}), estimated from the position of the low-angle peak is in the range of 9.8–10.4 nm. The unit cell parameter calculated using the equation $a = 2d_{100}/\sqrt{3}$ (11.3–11.9 nm) is in good agreement with the values reported by others [16–18].

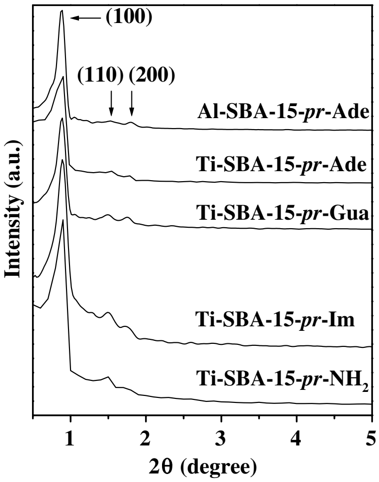

Fig. 1. Low-angle XRD profiles of modified SBA-15 materials.

3.1.2. TEM

The transmission electron micrographs (TEM) of the functionalized SBA-15 materials viewed through different orientations (Fig. 2) clearly reveal the 2D hexagonal pore arrangement and the long-range mesopore architecture. It may be noted that the long-range mesoporous-ordering characteristic of good-quality SBA-15 materials (see curved ordered features in TEM; Fig. 2) is not disturbed due to metal incorporation and organic-functionalization.

3.1.3. Surface area

All the catalysts showed type IV nitrogen adsorption–desorption isotherms with H1 hysterisis (Fig. 3). The textural properties of the materials are listed in Table 1. On introducing acid–base functionalities a marked decrease in specific surface area (S_{BET}), pore volume and average pore diameter was observed. The discrepancies between the pore diameters determined by sorption experiments and by TEM (Table 1) arise since the BJH method tends to underestimate pore diameters.

3.1.4. Chemical composition

The Si/Ti and Si/Al contents in metal ion-incorporated SBA-15 materials were found (XRF and EDAX) to be 40 and 22, respectively (Table 1). The organic composition (C, H & N) was estimated by elemental analysis. The amount of the functionalized base was estimated to be 0.8–2.5 mmol/g SBA-15 (Table 1). As expected, the amount functionalized varied with the size of the organic base. In the case of metal-incorporated materials, the amount of functionalized organic base is lower than that in the materials containing no Ti or Al ions.

3.1.5. FT-IR

FT-IR spectroscopy provided clear evidence for metal incorporation and organo-functionalization (Fig. 4(a) and (b)). SBA-15 showed a broad band in the NIR region 3200–3700 cm^{-1}. The IR peaks at 3325, 3300 and 3124 cm^{-1} (Fig. 4(a)), are probably due to the N–H stretching modes [20,21] of the functionalized-adenine and guanine. While, in principle, they can also correspond to the overtones of the bands in the range 1400–1800 cm^{-1}, this is unlikely, since in such a case they should be observed also for the imidazole-functionalized materials. Their absence in the spectrum of the latter indicates that they arise from the N–H stretching modes of the adenine/guanine groups. In the case of imidazole, the hydrogen of secondary NH is used-up during anchoring covalently to the SBA-15 surface. Hence, the imidazole-functionalized materials contained no NH group that can be seen in the NIR spectrum (Fig. 4(a)). Characteristic peaks due to C–H stretching vibrations (of propyl spacer, Im, Gua and Ade) appeared at 2857 and 2930 cm^{-1} [21]. Further, evidence for the presence of the organic bases was obtained from the sharp, characteristic peaks in the mid-IR region (Fig. 4(b)). It should be noted that these peaks are absent in non-functionalized SBA materials. While the band at 1557 cm^{-1} (for Ti-SBA-15-*pr*-Gua) and 1600 cm^{-1} (for Ti-SBA-15-*pr*-Ade) correspond to azomethine (C=N) group, the band at 1700 cm^{-1} present only in the case of Ti-SBA-15-*pr*-Gua corresponds to the C=O group of guanine. The rest of the bands (marked in Fig. 4(b)) are due to ring and skeletal vibrations [21]. Adenine and other bases could not be deposited directly by impregnation on the unsilynated SBA-15 surface as it leached out during Soxhlet extraction with DMF and CH_3CN. In this case, the IR spectrum of the solid after the extraction did not detect adsorbed adenine. In other words, in the absence of –Cl groups of the 3-chloropropyltriethoxysilane, the adenine and the other bases could not be anchored. The –NH group of adenine, guanine and imidazole reacts with the –Cl, forming N–C bonds and eliminating HCl in the process.

3.1.6. UV–Vis DRS

Pure adenine showed two characteristic UV bands at 244 and 288 nm due to π–π^* and n–π^* transitions. Adenine in SBA-15-*pr*-Ade, Ti-SBA-15-*pr*-Ade and Al-SBA-15-*pr*-Ade showed only one electronic band at 265 nm (Fig. 4(c)). Similarly, pure guanine showed UV bands at 247 and 294 nm. However, SBA-15-*pr*-Gua and Ti-SBA-15-*pr*-Gua, showed these bands at 250 and 302 nm. The charge transfer band at 211 nm (Fig. 4(c)) corresponds, probably, to dispersed-tetrahedral Ti and Al ions.

3.1.7. Thermal analysis

The thermal stability of the functionalized SBA-15 materials was estimated using thermogravimetric analysis. SBA-15 showed, mainly, two stages of weight loss: Stage I (308–473 K, 8.1 wt%) is due to desorption of adsorbed water and stage II (573–1073 K, 5.3 wt%) is due to decomposition of silanol groups (2Si–OH → Si–O–Si + H_2O). In the case of Ti-SBA-15, the weight losses in stages I and II are 4.6 and 4.4 wt%, respectively. Pure adenine decomposed in the temperature range 483–618 K. Functionalized

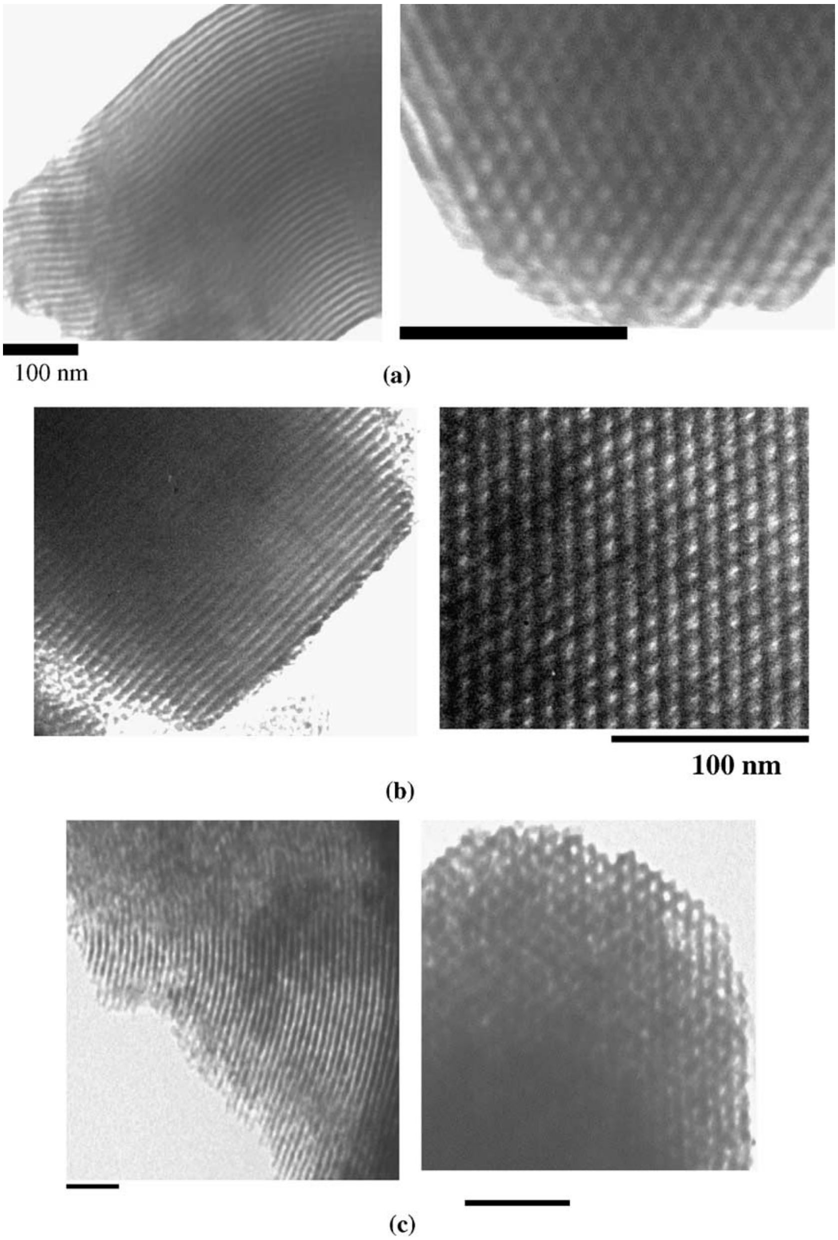

Fig. 2. TEM of (a) SBA-15, (b) Ti-SBA-15-*pr*-Ade and (c) Al-SBA-15-*pr*-Ade.

SBA-15 materials showed three stages of weight loss (Table 2). As in the case of unsilynated samples, stage I, in the silynated samples, is also due to desorption of adsorbed water. Stages II and III (in functionalized materials ca., SBA-15-*pr*-NH_2 and SBA-15-*pr*-Ade) are attributed to decomposition of functionalized organic matter (base NH_2/Ade and propyl group, respectively). Stage III has contribution also from the silanol groups. In an independent analysis (by C, H & N), we have also estimated the amount of organic base (from C, H, & N content) (Table 1). From the total weight loss (TG-DTG) and base content (C, H & N), the decomposed silanol groups, contributing to stage III, were determined (Table 2) and these are in the range expected for the mesoporous materials [22]. The functionalized organic base is thermally stable at least up to 473 K.

3.2. Surface acidity and basicity

The acid–base properties of the functionalized SBA-15 materials were investigated by TPD (Fig. 5) and DRIFT spectroscopy (Fig. 6). Surface acidity was estimated using NH_3 and pyridine as probe molecules. SBA-15 showed two desorption maxima (T_{max}) at 360 and 515 K in NH_3-TPD measurements (Fig. 5(i)). In the case of titanated materials, the desorption peak at 360 K disappeared and instead, two additional desorption maxima appeared at 390 and 435 K indicating the higher acidity of Ti-SBA-15. There is also an increase in the amount of NH_3 desorbed on going from SBA-15 to Ti-SBA-15 (0.34–0.9 mmol/g). Al-SBA-15 and Al-SBA-15-*pr*-Ade showed the desorption maximum at 390 K. The amount of NH_3

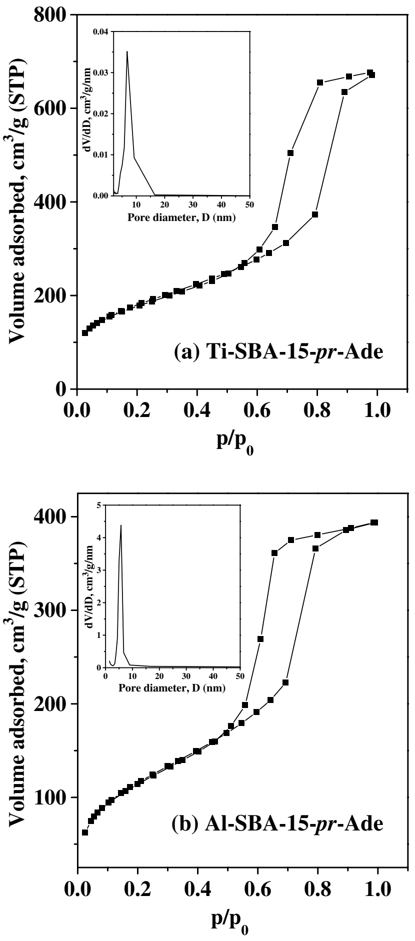

Fig. 3. Nitrogen adsorption–desorption isotherms.

desorbed from these samples is 0.81 and 0.77 mmol/g, respectively. Before adsorbing NH_3, the samples were activated at 473 K for 1 h. Thermogravimetric data (Section 3.1.7) indicate that all the adsorbed water in both the micro and mesopores would have desorbed during this activation process. Hence, the desorption peaks observed at 360, 390 and 435 K in NH_3-TPD experiments (Fig. 5(i)) are likely to be due to NH_3 only.

The spectra of pyridine adsorbed on SBA-15 and titanated SBA-15 samples clearly reveal the absence of Brönsted (1546 and 1639 cm^{-1}) and strong Lewis (1623 and 1455 cm^{-1}) acid sites (Fig. 6) [22–26]. Only weak Lewis acid sites (1577 and 1488 cm^{-1}) and H-bonded pyridine sites (1595 and 1444 cm^{-1}) were present. In Al-containing samples (Al-SBA-15, for example) the IR peaks corresponding to Lewis acid sites shifted marginally to 1580 and 1487 cm^{-1} (Fig. 6(a)), indicating that these samples are more acidic than Ti-containing samples. A weak, additional peak at 1547 cm^{-1} attributable to Brönsted acid sites is also observed in Al-containing samples (Fig. 6(a)). Fig. 6(b) and (c) illustrate the expected decrease in the intensity of adsorbed pyridine at higher temperatures. While the pyridine peaks associated with the Lewis acid sites had almost disappeared at around 473 K in the case of Ti-SBA-15, they were present, in significant intensity, in Al-SBA-15 (Fig. 6(b) and (c)). The intensity of the pyridine peaks is, in general, more in Al- than Ti-containing samples. This is in agreement with the metal ion content (Si/Al = 22 and Si/Ti = 40) as well as stronger acidity of Al than Ti. "Bare" SBA-15 did not possess any Brönsted or Lewis acid sites. The silanol groups on SBA-15 surface, which are known to be slightly acidic, showed IR peaks typical of H-bonded pyridine. The IR spectra reveal that Ti incorporation generated only weak Lewis acid sites and Al incorporation, on the other hand, generated both Brönsted and Lewis acid sites. In NH_3-TPD studies of Ti- and Al-containing samples, the peak at 390 K (Fig. 5(i)) is attributed to NH_3 bound to Lewis acid sites

Table 1
Physicochemical properties of SBA-15 materials

Material	Si/M output mol ratio (XRF/ EDAX)	Organic amine (mmol/g material)[a]	Elemental analysis (wt%)			XRD analysis		S_{BET} (m^2/g)	Pore volume (cm^3/g)			Pore diameter (nm)[b]	Wall thickness (nm)
			C	H	N	d_{100} (nm)	Unit cell parameter (nm)		Total	Mesopore	Micropore		
SBA-15	–	–	0.5	1.5	0	9.8	11.3	871	1.55	1.44	0.11	7.2	4.1
Ti-SBA-15	40	–	0.6	1.7	0	10.3	11.8	662	1.07	0.99	0.08	6.5 (8.0)	5.3
Al-SBA-15	22	–	0.3	0.7	0	10.4	11.9	808	1.15	1.0	0.15	5.7 (7.9)	6.2
SBA-15-*pr*-NH_2	–	2.5	10.2	1.9	3.4	10.0	11.5						
Ti-SBA-15-*pr*-NH_2	40	2.2	10.2	2.3	3.1	9.8	11.3	615	1.04	0.98	0.06	6.7	4.6
SBA-15-*pr*-Im	–	2.3	12.2	1.4	5.5	10.0	11.5						
Ti-SBA-15-*pr*-Im	40	1.9	11.9	1.2	5.4	9.9	11.4	432	0.65	–	–	6.1	5.3
SBA-15-*pr*-Gua	–	1.1	11.9	1.4	7.9	10.1	11.6						
Ti-SBA-15-*pr*-Gua	40	1.0	11.5	1.4	6.8	10.0	11.5						
SBA-15-*pr*-Ade	–	1.3	11.3	1.5	7.7	10.0	11.5						
Ti-SBA-15-*pr*-Ade	40	0.9	10.7	1.3	6.4	10.0	11.5	627	1.04	0.96	0.08	6.7 (7.6)	4.3
Al-SBA-15-*pr*-Ade	22	0.8	8.9	2.1	6.0	10.0	11.5	426	0.66	0.64	0.02	5.7 (7.5)	4.8

[a] Values estimated from C, H & N analysis.
[b] Pore diameter was determined using the BJH model. Values in parentheses are those estimated from TEM.

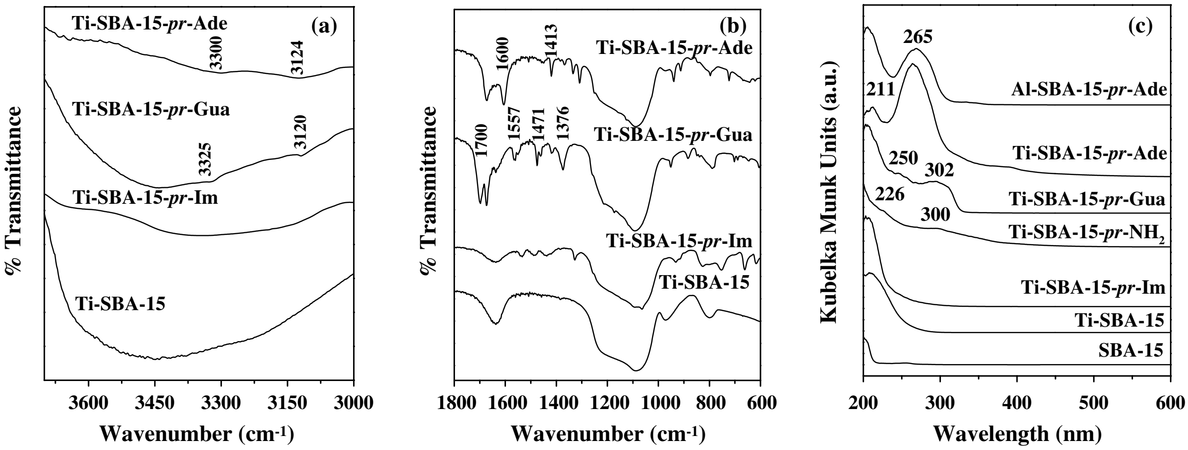

Fig. 4. (a) Near-IR, (b) Mid-IR and (c) UV–Vis DRS spectra of SBA-15 materials.

Table 2
Thermal and elemental analysis of functionalized SBA-15 materials

Material	Stage no.	Temperature region (K)	Weight loss (%)	Assignment for weight loss	N-content (mmol/g silica)	Concentration of H_2O/Si–OH Desorbed/decomposed (mmol/g silica)[b]
SBA-15	I	308–473	8.1	Desorption of physisorbed/chemisorbed water	–	4.5 (H_2O)
	II	573–1073	5.3	Decomposition/condensation of silanol groups (2Si–OH → Si–O–Si + H_2O)	–	5.8 (Si–OH)
SBA-15-*pr*-NH_2	I	308–375	5.4	Desorption of physisorbed/chemisorbed water	–	3.0 (H_2O)
	II	375–530		Decomposition organic functional group (propyl amine) and silanol groups	2.5	3.8 (Si–OH)
	III	530–862	17.1[a]			
“Neat” adenine	I	483–618	100.0	Decomposition of adenine	–	–
SBA-15-*pr*-Ade	I	308–463	5.7	Desorption of physisorbed/chemisorbed water	–	3.2 (H_2O)
	II	463–607		Decomposition organic functional group (propyl adenine) and silanol groups	1.3	5.6 (Si–OH)
	III	607–848	25.0[a]			
Ti-SBA-15	I	308–473	4.6	Desorption of physisorbed/chemisorbed water	–	2.5 (H_2O)
	II	573–1073	4.4	Decomposition/condensation of silanol groups	–	4.8 (Si–OH)

[a] Refers to the total weight loss in stages II and III.

[b] Values are estimated from the total weight loss in thermal analysis and the functionalized organic base content estimated from C, H & N analysis.

and the one at 435 K to NH_3 associated with the surface –OH groups through H-bonding interactions. Both TPD and DRIFT studies also reveal that organo-functionalization does not influence the Lewis acidity of Ti and Al sites.

The type of Al coordination in Al-SBA-15 and Al-SBA-15-*pr*-Ade was probed using ^{27}Al MAS NMR (Fig. 7). The Al-containing samples showed a NMR peak at around 53 ppm attributable to Al in a tetrahedral environment

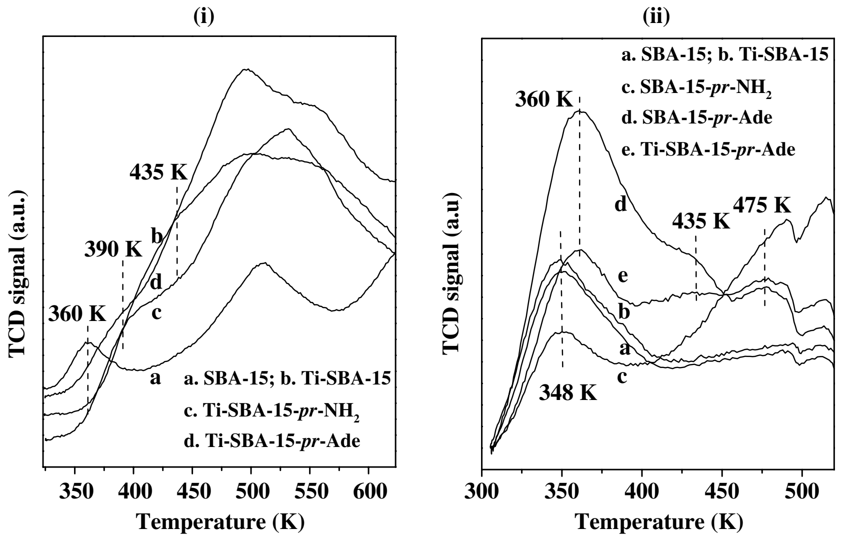

Fig. 5. (i) NH_3-TPD and (ii) CO_2-TPD profiles of SBA-15 materials.

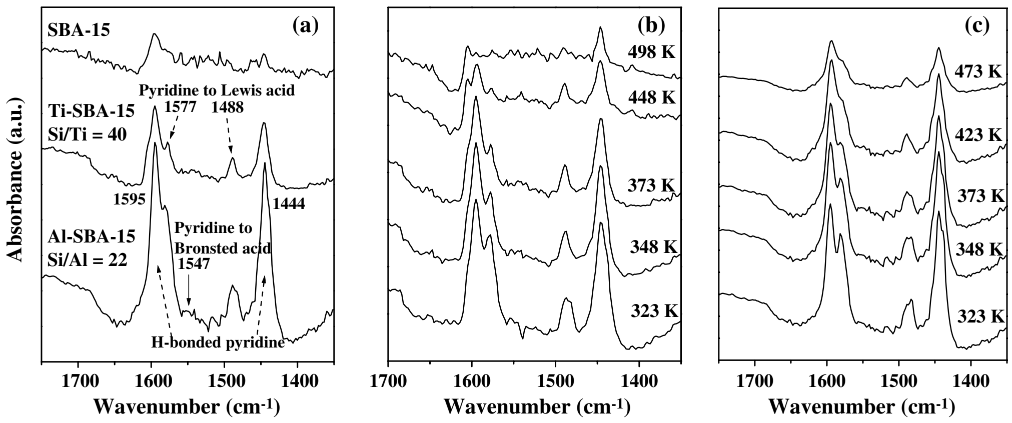

Fig. 6. DRIFT spectra of adsorbed pyridine: (a) on SBA-15, Ti-SBA-15 and Al-SBA-15 at 373 K and normalized spectral intensity, (b) on Ti-SBA-15 at different temperatures, and (c) on Al-SBA-15 at different temperatures.

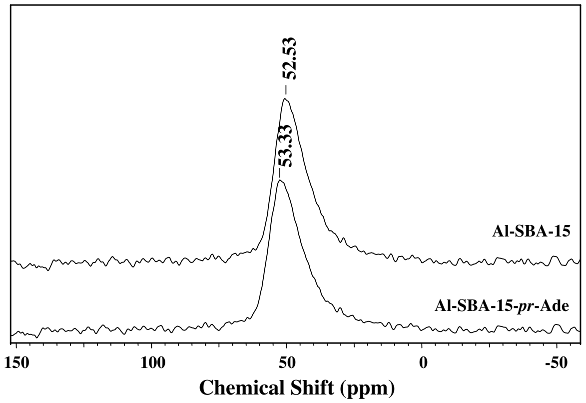

Fig. 7. ^{27}Al MAS NMR of Al-SBA-15 and Al-SBA-15-*pr*-Ade.

bound covalently to four –OSi groups [17,22–26]. The absence of a NMR peak at 0 ppm indicates that all the aluminium atoms are exclusively in tetrahedral coordination and no octahedral Al ions are present. The Brönsted and Lewis acidity of these samples is due to the framework incorporated tetrahedral Al.

Surface basicity was studied by adsorption of CO_2, an "acidic" molecule (Fig. 5(ii)). "Bare" SBA-15 and Ti-SBA-15 showed a desorption peak at 348 K in CO_2-TPD. In SBA-15-*pr*-NH_2, the intensity of the desorption peak at 348 K decreased and an additional desorption peak appeared at 475 K. The latter is, possibly, due to CO_2 chemisorbed on the amine function (–NH_2). In adenine-functionalized materials, CO_2 desorption occurred at 435 K and 360 K. These desorptions are attributed to CO_2 chemisorbed at the secondary (NH) and tertiary amine functions in adenine, respectively. The shift in T_{max} to higher temperatures compared to that in SBA-15 and Ti-SBA-15 clearly indicates that amine-functionalization, as expected, enhances surface basicity. CO_2 uptake was similar (around 2.9 mmol/g of catalyst) for both SBA-15 and Ti-SBA-15. When the amine functions were grafted on the surface, the amount of CO_2 adsorbed increased to 3.8

(for SBA-15-*pr*-NH_2 and Ti-SBA-15-*pr*-NH_2), 4.3 (for SBA-15-*pr*-Ade) or 5.3 mmol of CO_2/g of catalyst (for Ti-SBA-15-*pr*-Ade), respectively. In terms of mmoles of CO_2 adsorbed *per mole of grafted amine molecule,* the values for the above four catalysts were 0.9, 1.0, 1.4 and 2.4, respectively. The TPD data indicate that the binding energy of CO_2 to different amines decreases in the order: primary amine > secondary amine > tertiary amine.

3.3. Sites for CO_2 activation

In our earlier study [14] we had found that Ti-SBA-15-*pr*-Ade exhibits superior catalytic activity, compared to Ti-SBA-15-*pr*-NH_2, for cyclic carbonates synthesis from epoxides and CO_2. In the present study, the active sites for CO_2 activation have been characterized using in situ DRIFT spectroscopy. The solid samples were heated to 373 K and exposed to CO_2 at 253–298 K for 1 h. DRIFT spectra of the samples were recorded before and after CO_2 exposure. The difference spectrum yielded spectral features due to adsorbed CO_2. No new IR peaks were detected in the difference IR spectrum of “bare” SBA-15, Ti-SBA-15 and Al-SBA-15. There was no significant activation of CO_2 on these samples. The organo-functionalized SBA-15 materials showed *new* IR peaks due to CO_2 activated at the basic sites (–NH_2, Im, Gua and Ade). Representative DRIFT spectra of activated CO_2 on Ti- and Al-containing materials are shown in Fig. 8.

Metal complexes, metal oxides and zeolites are known to activate CO_2 and form a variety of activated CO_2 complexes (terminal and bridged) [3,4,27–30]. CO_2 exhibits different types of coordination modes—η^1(O), η^1(C) and η^2(C, O) (Scheme 1) [3,4,7]. CO_2 molecules can be activated at the carbon atom if the active site (M) is electron-rich or through the oxygen atom if M is electron-deficient. IR spectroscopy can differentiate these coordination modes of CO_2. The DRIFT spectra (Fig. 8) reveal that CO_2 was activated through η^1(C)-type coordination on organo-functionalized SBA-15 materials. Several new peaks were observed in the range 1250–1700 cm^{-1}. Amines upon reaction with CO_2 form carbamate species [6,31,32]. The latter are in equilibrium with the carbamic acid species (Scheme 2). DRIFT peaks at 1609 and 1446 cm^{-1} (Fig. 8) are due to these surface carbamate species [30]. These carbamate species react with adsorbed water or surface hydroxyl groups forming product carbonates, bicarbonates or formates. Formation of all these forms of CO_2 species on SBA-15 surfaces is apparent from the DRIFT spectra (Fig. 8). The peak at 1345 cm^{-1} arises due to monodentate carbonates and that at 1380 cm^{-1} is due to the bidentate carbonate species. The peaks at 1420 and 1650 cm^{-1} are due to the monodentate and bidentate bicarbonates species, respectively [27–30].

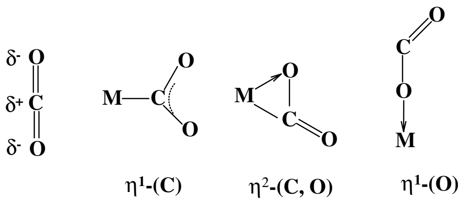

Scheme 1.

In the IR spectra of adenine- and guanine-functionalized SBA-15, the peaks at 1609 and 1446 cm^{-1} (due to the activated CO_2 species—carbamate) are more pronounced and sharper than those due to carbonates, bicarbonates and formates. These peaks are less intense for propyl amine-functionalized SBA-15 and are barely seen for the Im-functionalized materials. It may be recalled from CO_2-TPD results (Section 3.2) that the T_{max} for CO_2 desorption from primary amine-functionalized SBA-15 is higher (475 K)

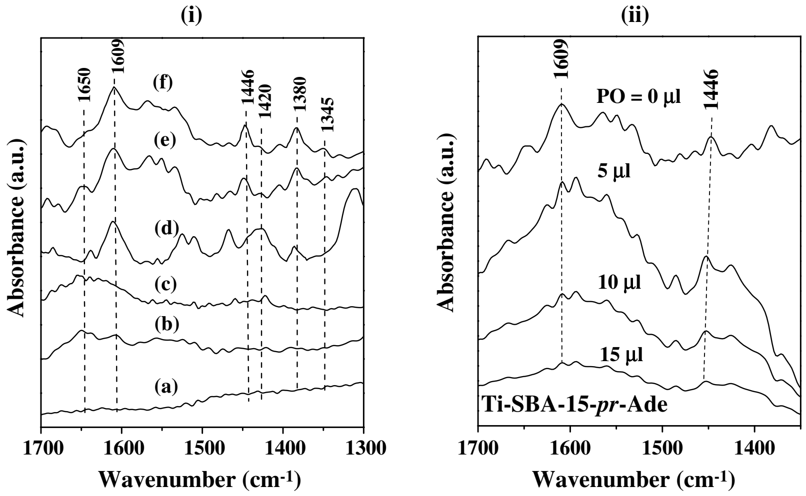

Fig. 8. (i) DRIFT spectra of activated CO_2: (a) Ti-SBA-15, (b) Ti-SBA-15-*pr*-NH_2, (c) Ti-SBA-15-*pr*-Im, (d) Ti-SBA-15-*pr*-Gua, (e) Ti-SBA-15-*pr*-Ade, and (f) Al-SBA-15-*pr*-Ade, and (ii) DRIFT spectra showing the spectral changes of activated CO_2 on Ti-SBA-15-*pr*-Ade upon contacting with propene oxide (PO).

(a) CO_2 activation at primary amines:

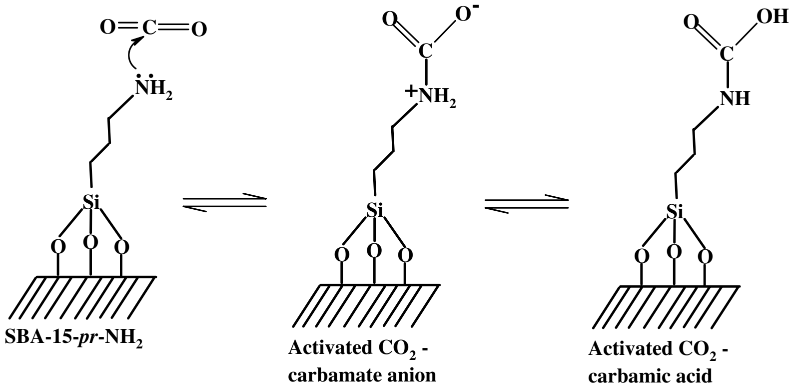

(b) CO_2 activation at secondary amines:

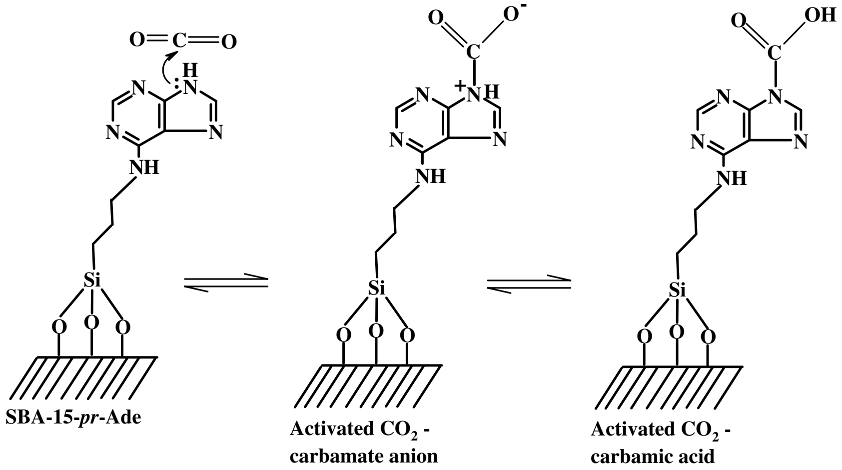

(c) CO_2 activation at tertiary amines:

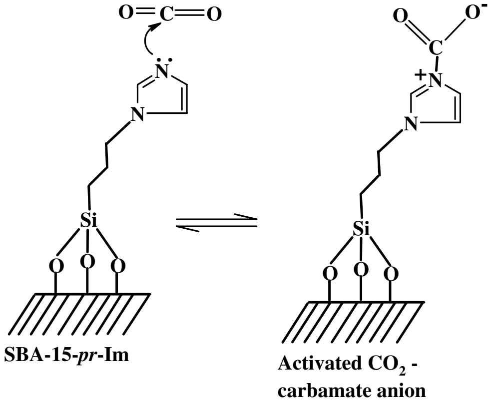

Scheme 2.

than that for secondary ($T_{max} = 435$ K) and tertiary ($T_{max} = 360$ K) amines. However, the stability of surface carbamates formed on the different amines follows the reverse trend: tertiary < secondary < primary. This is because the primary and secondary amines can form carbamate anions, which exist in equilibrium with the corresponding carbamic acid species (Scheme 2). Such an equilibrium is not possible for carbamate anions formed on tertiary amines since there is no H-atom attached to the tertiary N atom. Hence, the lifetime of a carbamate species formed on tertiary amines is relatively shorter. As a consequence, their IR peaks are not detected (see for example the IR spectrum of Im-functionalized materials) (Fig. 8(i)).

The intensity of the IR peaks due to the various activated CO_2 species increased with CO_2 pressure (2–20 bar)

[14]. The IR peaks are more intense at lower temperatures due to the higher concentration of the adsorbed CO_2 and increased stability of the corresponding carbamate species at lower temperatures [14]. The intensity of the surface carbamate peaks (1609 and 1446 cm^{-1}, respectively) decreased on the addition of propene oxide (Fig. 8(ii)) due to formation of cyclic carbonates.

Non-grafted spacers and reactive compounds had been completely removed from the SBA-15 surface ensuring that the catalytic reactions take place only on surface-grafted species. The spacer molecules have three potential sites, which can bind to the silica surface. While all the three Si–O–Et can, in principle, react with surface silanol groups to form Si–O–Si bonds, as suggested in Scheme 2, it is also likely that only one or two of the ethoxy groups would react with surface silanol groups. In addition, two of the X-propyltriethoxysilane molecules (X = 3-chloro or 3-amino) may also react with each other forming direct Si–O–Si bonds between the spacer molecules.

3.4. Catalytic activity—cycloaddition of CO_2 to epoxides

Cycloaddition of CO_2 to chloropropene oxide yielded chloropropene carbonate as the main product; diols and ethers also formed in minor amounts. "Bare" SBA-15 was only weakly active and cyclic carbonate selectivity was very low (Table 3, entry no. 1). Upon titanation (Ti-SBA-15) the activity as well as cyclic carbonate selectivity increased (from 59% for SBA-15 to 86.3%) (see entry no. 2; Table 3). Amine-functionalization enhanced the catalytic activity significantly. This enhancement increased in the order: –Im < $–NH_2$ < –Gua < –Ade. A synergistic enhancement in catalytic activity was observed when Ti and amine were both present on SBA-15. Al-SBA-15-*pr*-Ade was superior to Ti-SBA-15-*pr*-Ade. In contrast to all the earlier solid catalysts, including the commercial processes, wherein a significant amount of solvent (CH_2Cl_2) is used in the synthesis of cyclic carbonates, the present catalysts are highly active and selective, even in the absence of any solvent and co-catalyst/promoters (Table 3). The reaction occurs at mild conditions (6.9 bar, 393 K) and shorter contact times (3–4 h). Styrene carbonate was also synthesized in high yields and selectivity over amine-functionalized Ti- or Al-SBA-15 catalysts (Table 4). Adenine and guanine-functionalized catalysts were superior to imidazole-functionalized Ti-SBA-15. Activity was higher when Lewis acid (Ti, Al) and Lewis base (adenine, guanine) were both present.

Table 3
Chloropropene carbonate synthesis over inorganic–organic mesoporous SBA-15 materials utilizing CO_2

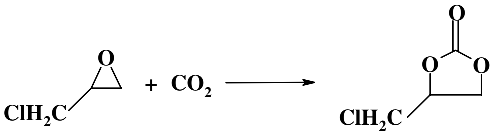

Run no.	Catalyst	Acidic site	Basic site	Epoxide conversion, %	Cyclic carbonate selectivity, %[a]
1	SBA-15	–	(OH, H_2O)	15.8	59.0
2	Ti-SBA-15	Ti	(OH, H_2O)	20.1	86.3
3	Al-SBA-15	Al	(OH, H_2O)	22.1	92.2
4	SBA-15-*pr*-NH_2	–	$–NH_2$	35.8	87.7
5	Ti-SBA-15-*pr*-NH_2	Ti	$–NH_2$	50.5	88.7
6	SBA-15-*pr*-Im	–	Im	23.2	80.6
7	Ti-SBA-15-*pr*-Im	Ti	Im	31.7	93.9
8	SBA-15-*pr*-Gua	–	Gua	69.0	85.8
9	Ti-SBA-15-*pr*-Gua	Ti	Gua	81.3	93.5
10	SBA-15-*pr*-Ade	–	Ade	80.5	75.0
11	Ti-SBA-15-*pr*-Ade	Ti	Ade	93.9	89.1
12	Al-SBA-15-*pr*-Ade	Al	Ade	98.1	89.1

Reaction conditions: catalyst (100 mg), epoxide (18 mmol), P_{CO_2} (6.9 bar), temperature (393 K), reaction time (4 h).

[a] Balance includes diols and ethers.

Even though, the cycloaddition reaction could be carried out in the absence of any solvent over these catalysts with high conversions and selectivities, the use of solvents prolonged catalyst life significantly. The catalyst was not deactivated even after the tenth recycle. We had, earlier, found [14] that one of the main roles of the solvent is to continuously remove carbonaceous deposits from the catalyst surface and keep it clean. No leaching of Ti and amine functionality during the experiment was detected [14].

A correlation between the intensity of the IR peak at 1609 cm^{-1} for activated CO_2 species (carbamate anion) and cyclic carbonate yield has been observed (Fig. 9). Interestingly, a plot of CO_2 desorption temperature (T_{max}) versus chloropropene carbonate yield (mol%) shows a "volcanic plot" variation (Fig. 10). The plot reveals that SBA-15 samples containing tertiary and primary amines

Table 4
Styrene carbonate synthesis utilizing CO_2: catalytic activity of inorganic–organic mesoporous SBA-15 materials

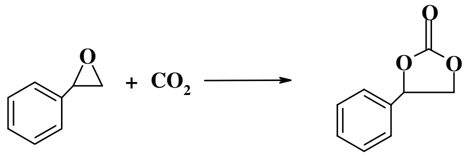

Run no.	Catalyst	Acidic site	Basic site	Epoxide conversion, %	Cyclic carbonate selectivity, %[a]
1	SBA-15-*pr*-Im	–	Im	18.7	95.5
2	Ti-SBA-15-*pr*-Im	Ti	Im	28.2	97.9
3	SBA-15-*pr*-Gua	–	Gua	82.4	97.5
4	Ti-SBA-15-*pr*-Gua	Ti	Gua	97.9	97.1
5	SBA-15-*pr*-Ade	–	Ade	86.4	97.2
6	Ti-SBA-15-*pr*-Ade	Ti	Ade	94.0	94.6
7	Al-SBA-15-*pr*-Ade	Al	Ade	98.4	97.9

Reaction conditions: catalyst (100 mg), epoxide (18 mmol), P_{CO_2} (6.9 bar), temperature (393 K), reaction time (8 h).

[a] Balance includes diols and ethers.

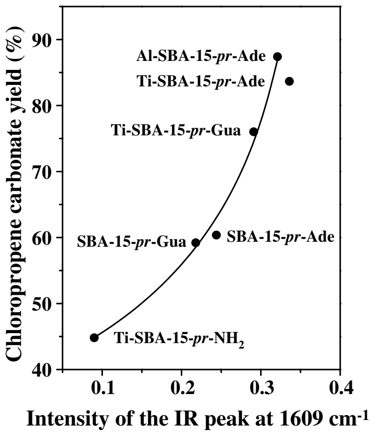

Fig. 9. Correlation between chloropropene carbonate yield (mol%) and intensity of IR peak at 1609 cm^{-1} of activated CO_2.

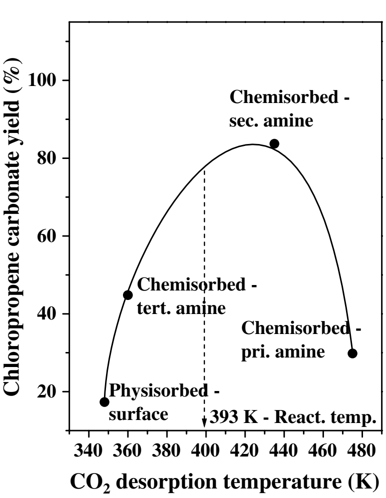

Fig. 10. Correlation between chloropropene carbonate yield (mol%) and CO_2 desorption peak maximum (T_{max}) of SBA-15 samples functionalized with different amines.

are less active than secondary amines in cyclic carbonates synthesis. There is hence, an optimal value in the binding of CO_2 to the active sites. Basic sites wherein CO_2 is held either weakly (tertiary N atoms) or too strongly (primary amines) are less active than those with an intermediate strength of binding of CO_2 (secondary amines). Figs. 9 and 10, therefore, indicate the density of basic sites of medium strength is a crucial parameter in the design of solid catalysts for the cycloaddition reaction.

4. Conclusions

An investigation of the active sites for CO_2 activation and utilization in cyclic carbonate synthesis over SBA-15, functionalized with Lewis acids (Ti^{4+} and Al^{3+}) and bases ($-NH_2$, guanine, adenine and imidazole) containing primary, secondary and tertiary amines, is reported. The bases were covalently anchored on the silynated surfaces. The acid–base properties of the materials were determined by TPD and DRIFT spectroscopy using NH_3 and pyridine as probe molecules for the acid sites and CO_2 for the basic sites. The amine-functionalized Ti/Al-SBA-15 materials were found to be efficient catalysts for the synthesis of chloropropene and styrene carbonates from the corresponding epoxides and CO_2 at mild conditions (6.9 bar, 393 K, 3–8 h) without using any solvent or promoters/co-catalysts. Samples containing adenine were more efficient. All the amine-functionalized samples activate CO_2 and form surface carbamate anion species whose concentration correlates well with cyclic carbonate yields. The stability of the activated CO_2 complex formed on the basic amine sites on the surface decreases in the order: primary > secondary > tertiary. There is an optimal dependence (“volcanic plot”) of the cyclic carbonate yield on the desorption temperature (T_{max}) of CO_2. Sites with intermediate basicity (secondary amines) are more active than those wherein CO_2 is held either too weakly (tertiary N atoms) or too strongly (primary N atoms).

Acknowledgements

R.S. acknowledges Council of Scientific and Industrial Research (CSIR), New Delhi for a fellowship. Authors thank Dr. K.V.R. Chary, IICT, Hyderabad for the help in TPD measurements. This work forms a part of the Network project “Catalysts and Catalysis” (P23-CMM005.3) sponsored by CSIR, New Delhi.

References

[1] M.M. Halmann, Chemical Fixation of Carbon Dioxide—Methods for Recycling CO_2 into Useful Products, CRC Press, Boca Raton, FL, 1993.
[2] D.J. Darensbourg, M.W. Holtcamp, Coord. Chem. Rev. 153 (1996) 155.
[3] D.H. Gibson, Chem. Rev. 96 (1996) 2063.
[4] M. Aresta, I. Tommasi, Energy Convers. Manage. 38 (1997) S373.
[5] X. Yin, J.R. Moss, Coord. Chem. Rev. 181 (1999) 27.
[6] S. Inoue, N. Yamazaki (Eds.), Organic and Bio-organic Chemistry of Carbon Dioxide, Kodansha Ltd., A Halsted Press Book, John Wiley & Sons, Tokyo, Japan, New York, 1982.
[7] D.A. Palmer, R. van Eldik, Chem. Rev. 83 (1983) 651.
[8] Y. Li, X.-Q. Zhao, Y.-J. Wang, Appl. Catal. A: General 279 (2005) 205.
[9] R. Srivastava, D. Srinivas, P. Ratnasamy, Catal. Lett. 89 (2003) 81.
[10] R. Srivastava, D. Srinivas, P. Ratnasamy, Catal. Lett. 91 (2003) 133.
[11] R. Srivastava, D. Srinivas, P. Ratnasamy, Stud. Surf. Sci. Catal. 154 C (2004) 2703.
[12] R. Srivastava, M.D. Manju, D. Srinivas, P. Ratnasamy, Catal. Lett. 97 (2004) 41.
[13] R. Srivastava, D. Srinivas, P. Ratnasamy, Appl. Catal. A: General 289 (2005) 128.
[14] R. Srivastava, D. Srinivas, P. Ratnasamy, J. Catal. 233 (2005) 1.
[15] D. Zhao, J. Feng, Q. Huo, N. Melosh, G.H. Fredrickson, B.F. Chmelka, G.D. Stucky, Science 279 (1998) 548.
[16] P. Wu, T. Tatsumi, T. Komatsu, T. Yashima, Chem. Mater. 14 (2002) 1657.
[17] A. Vinu, V. Murugesan, W. Böhlmannn, M. Hartmann, J. Phys. Chem. B 108 (2004) 11496.

[18] P. Sutra, D. Brunel, Chem. Commun. (1996) 2485.
[19] X.-G. Zhou, X.-Q. Yu, J.-S. Huang, S.-G. Li, L.-S. Li, C.-M. Che, Chem. Commun. (1999) 1789.
[20] K. Nakamoto, Infrared and Raman Spectra, fourth ed., Wiley, New York, 1986.
[21] A.S. Maria Chong, X.S. Zhao, J. Phys. Chem. B 107 (2003) 12650.
[22] A. Taguchi, F. Schüth, Micropor. Mesopor. Mater. 77 (2005) 1.
[23] B. Chakraborty, B. Viswanathan, Catal. Today 49 (1999) 253.
[24] M. Hunger, U. Schenk, M. Breuninger, R. Gläser, J. Weitkamp, Micropor. Mesopor. Mater. 27 (1999) 261.
[25] L.Y. Chen, Z. Ping, G.K. Chuah, S. Jaenicke, G. Simon, Micropor. Mesopor. Mater. 27 (1999) 231.
[26] A. Corma, V. Fornés, M.T. Navarro, J. Pérez-Pariente, J. Catal. 148 (1994) 569.
[27] F. Solymosi, H. Knözinger, J. Catal. 122 (1990) 166.
[28] K. Tomishige, Y. Ikeda, T. Sakaihori, K. Fujimoto, J. Catal. 192 (2000) 355.
[29] K.T. Jung, A.T. Bell, J. Catal. 204 (2001) 339.
[30] A.C.C. Chang, S.S.C. Chuang, M. Gray, Y. Soong, Engery & Fuels 17 (2003) 468.
[31] E.R. Pérez, M. Odnicki da Silva, V.C. Costa, U.P. Rodrigues-Filho, D.W. Franco, Tetrahedron Lett. 43 (2002) 4091.
[32] E.F. da Silva, H.F. Svendsen, Ind. Eng. Chem. Res. 43 (2004) 3413.